Journal of Colloid and Interface Science 554 (2019) 344–352

Contents lists available at ScienceDirect

Journal of Colloid and Interface Science

journal homepage: www.elsevier.com/locate/jcis

Regular Article

Synthesis of green emissive carbon dots@montmorillonite composites and their application for fabrication of light-emitting diodes and latent fingerprints markers

Yuechen Zhai [a,b], Fangzhong Shen [c], Xutao Zhang [a,b], Pengtao Jing [a], Di Li [a], Xudong Yang [d], Ding Zhou [a,*], Xiaowei Xu [e,*], Songnan Qu [a,*]

[a] State Key Laboratory of Luminescence and Applications, Changchun Institute of Optics, Fine Mechanics and Physics, Chinese Academy of Sciences, Changchun 130033, PR China
[b] University of Chinese Academy of Sciences, Beijing 100049, PR China
[c] State Key Laboratory of Supramolecular Structure and Materials, College of Chemistry, Jilin University, Changchun 130012, PR China
[d] School of Chemical Engineering, Advanced Institute of Materials Science, Changchun University of Technology, Changchun 130012, PR China
[e] Department of Periodontology, School and Hospital of Stomatology, Jilin University, Changchun 130021, PR China

GRAPHICAL ABSTRACT

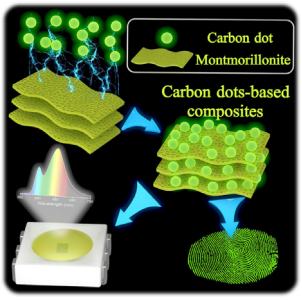

ARTICLE INFO

Article history:
Received 26 March 2019
Revised 7 July 2019
Accepted 8 July 2019
Available online 9 July 2019

Keywords:
Carbon dot
Montmorillonite
Solid-state luminescent materials
Light-emitting diodes
Latent fingerprint detection

ABSTRACT

Multifunctional solid-state luminescent materials are strongly desired in a wide variety of applications. In this work, green emissive carbon dots@montmorillonite (g-CDs@MMT) composites were synthesized based on green emissive carbon dots and MMT clays in a convenient method by embedding g-CDs into the MMT clays. Due to the confinement of g-CDs in the layered structure of the MMT clay matrix, g-CDs are uniformly dispersed in the resulting g-CDs@MMT solid-state composites. This efficiently prevents the aggregation-induced solid-state luminescence quenching of g-CDs, and a photoluminescence quantum yield of 11% could be achieved by the g-CDs@MMT composites under a 405 nm light. Additionally, the g-CDs@MMT composites exhibit low-toxicity, excellent thermal stability, photostability, resistance to organic solvents, and a small particle size. All of these advantages enable applications in fabricating white light-emitting diodes with different color temperatures, where the g-CDs@MMT composites are applied as the color conversion layer. Furthermore, by using the g-CDs@MMT composites as a fluorescence labeling marker, the latent fingerprint detection on a variety of object surfaces could be realized.

* Corresponding authors.
E-mail addresses: zhouding@ciomp.ac.cn (D. Zhou), xiaoweixu@jlu.edu.cn (X. Xu), qusn@ciomp.ac.cn (S. Qu).

https://doi.org/10.1016/j.jcis.2019.07.022
0021-9797/

1. Introduction

Luminescent materials play a significant and special role in human life, and have recently drawn increasing attention [1,2]. With scientific and technological developments, luminescent materials have been applied in many fields, such as sensing, lighting, display, and medical diagnostics [3–9]. In particular, multifunction solid-state luminescent materials are strongly desired in a wide variety of applications [6,10–12]. Until now, the reported luminescent materials have commonly focused on rare earth-doped nanoparticles, organic dyes, semiconductor quantum dots (QDs) and perovskite QDs [13–20]. However, these materials have some drawbacks, such as inability to be regenerated [21], weak thermostability [22] and potential toxicity of heavy metal elements [23–25].

In recent years, carbon dots (CDs) have been found to be one of the most significant luminescent materials due to their unique properties, including low toxicity [26–29], tunable emission [30,31], low cost [10,32–38], good biocompatibility [11,39–41], and high photostability [33,42,43], giving rise to their broad application field, such as in latent fingerprint detection [44] and light-emitting diodes (LEDs) [10,30,31,45,46]. Although CD-based latent fingerprint detection has been much reported, these achievements are mainly based on CD solutions [44]. With respect to solid-state labeling markers, the aqueous solutions lack portability and are difficult to preserve; moreover, the facile diffusion of the solution usually decreases the resolution of latent fingerprint detection when utilized to label fingerprints on paper and glass. In contrast, the solid-state labeling markers without diffusion can better show clear fingerprints by adhering to the residual human skin oil on the object surfaces [47]. Therefore, CDs are more functional in a solid-state powder format rather than in a suspension colloidal format. However, pure CD powders cannot be directly applied as fluorescent labeling markers because the agglomeration of pure CDs in the solid state can lead to serious photoluminescence (PL) quenching (i.e., aggregation-induced luminescence quenching) when isolated from the colloidal suspensions; this is mainly due to the non-radiative recombination caused by energy or charge transfer among the different luminescent centers or substances in CD aggregates [48–51]. In addition, the aggregation-induced luminescence quenching of CDs is also the main obstacle when CDs are applied as a color conversion layer in LEDs [31,52,53]. To overcome this problem, several organic and inorganic materials have been utilized to disperse the CDs and maintain the PL properties of CDs in the desired solid state, such as in silica, starch, or $BaSO_4$ [42,52,53]. However, the adhesive ability and pulverulent state of these CD-containing composites are not satisfactory or suitable for latent fingerprint detection as fluorescent labeling markers.

As low-toxicity, low-cost and superior matrix material, montmorillonite (MMT) clay has attracted significant attention as an inorganic filler material [54]. Several nanoparticles@MMT nanocomposites have been demonstrated by intercalating metal and semiconductor nanoparticles, including gold, platinum, CdS and CdTe nanoparticles [54]. However, CDs@MMT composites have not yet been reported, and their applications in latent fingerprint detection and LEDs have not been investigated.

In this work, based on green emissive carbon dots (g-CDs) with photoluminescence quantum yields (PLQYs) of 14% and MMT clays, green emissive composites are prepared by a convenient method. The association of g-CDs and MMT in preparing the g-CDs@MMT composites is based on multifactor interactions, including electrostatic attraction, hydrogen bonding and complexation. Due to the confinement of g-CDs in the layered structure of the MMT clay matrix, g-CDs are uniformly dispersed in the resulting g-CDs@MMT solid-state composites, which efficiently prevents the aggregation-induced solid-state luminescence quenching of g-CDs; the PLQYs of the g-CDs@MMT composites could reach 11% under a 405 nm light. The PLQY was slightly lower than that of g-CDs in aqueous solution due to the presence of a small number of metal cations in MMT. However, the g-CDs@MMT composites exhibit low toxicity, excellent thermal stability, photostability, resistance to organic solvent, and small particle sizes. Benefiting from these advantages, LEDs were fabricated that had different Commission International de L'Eclariage (CIE) coordinates and tunable color temperature based on 450 nm chips and the g-CDs@MMT composites, where the composites were applied as the color conversion layer. Additionally, by using the g-CDs@MMT composites as a fluorescence labeling marker, the latent fingerprint detection on a variety of object surfaces could be realized (Fig. 1).

2. Materials and methods

2.1. Materials

Urea (99%) was purchased from Maclin (Shanghai, China). Citric acid (99.5%) and montmorillonite clay (MMT, catalog number: M109698-100 g, purity: 99%) were purchased from Aladdin Ltd. (Shanghai, China). The encapsulating materials used were epoxy-silicon resin A and B (98%), which were purchased from Ausbond. The raw materials were not further purified before use.

2.2. Synthesis of green light-emitting carbon dots (g-CDs)

According to our previous work, the microwave-assisted heating method was used to prepare g-CDs. Three grams of citric acid and 6 g of urea were added to 20 mL of deionized water to form a transparent solution. The mixed solution was microwaved for 5 min in a domestic 650 W microwave oven for deep heating, during which the mixed solution changed in color and state from a colorless liquid to a dark brown solid, indicating the formation of g-CDs. The solid was dissolved in water and centrifuged twice at 8000 rpm for 5 min to remove the aggregated particles. Finally, the g-CD solution was obtained and freeze-dried for further use.

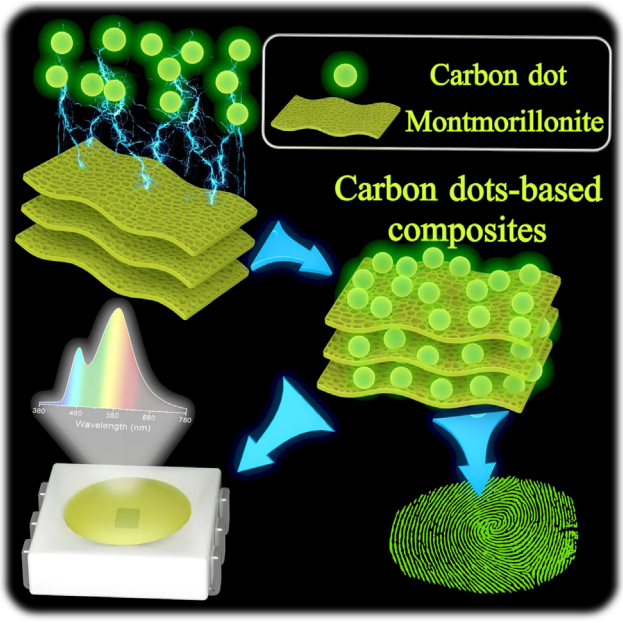

Fig. 1. Schematics of g-CDs@MMT composites preparation for WLEDs and the latent fingerprint detection.

2.3. Preparation of g-CDs@MMT composites

A 150 mg sample of g-CDs was dissolved in 20 mL of aqueous solution and underwent sonication for 5 min. Three grams of MMT clay were added to 30 mL of aqueous solution and stirred at 500 rpm for 5 min to form the MMT clay turbid liquid. Next, the prepared g-CDs aqueous solution was poured into the turbid liquid, and was stirred continuously for 30 min at 500 rpm. Finally, the g-CDs@MMT composites were obtained by filtering and were freeze-dried for further experiments and measurements. Composites with different g-CDs-to-MMT ratios and different reaction times were obtained via a similar procedure, but changing the g-CDs-to-MMT ratios or the reaction times.

2.4. Preparation of g-CDs@MMT-based luminescent bulk materials

Epoxy-silicone A and B (volume ratio: 2:1) were used to disperse the g-CDs@MMT composites. The mixture was continuously stirred for 10 min until the g-CDs@MMT composites were homogenously dispersed. To remove the air, the mixture was placed in a vacuum oven for vacuum treatment. The mixture was then poured into various molds and baked for 1 h at 60 °C, after which the various green emissive bulks were obtained.

2.5. Fabrication of light-emitting diodes (LEDs) from g-CDs@MMT composites

Indium gallium nitride (InGaN) microchips were placed at the bottom of an LED base, which emitted 450 nm light with a working voltage of 3.0 V. To form the color conversion layers, g-CDs@MMT composites were mixed with epoxy-silicone A and B at the different volume ratios of 8:3, 5:3 and 4:3. After vacuum treatment, the mixture were filled into the InGaN microchips and cured at 80 °C for 1 h. In this way, LEDs based on g-CDs@MMT composites were obtained.

2.6. Cytotoxicity assay of g-CDs, MMT and g-CDs@MMT composites

The cytotoxicity of g-CDs, MMT and g-CDs@MMT composites were evaluated by the 3-(4,5-dimethyl-2-thiazolyl)-2,5-diphenyl-2-H-tetrazolium bromide (MTT) assay. RAW264.7 cells were seeded at 5×10^3 cells per well in a 96-well plate and cultured overnight. Different concentration of g-CDs, MMT and g-CDs@MMT composites (0, 10, 20, 50, 100, 150, and 200 μg/mL) were then added to the corresponding wells. After 24 h of incubation, 20 μL of MTT (5 mg/mL) was added into each well and incubated for another 4 h at 37 °C. Finally, the medium was removed and 150 μL of dimethyl sulfoxide was added to each well to dissolve the formed purple precipitate. The absorbance was detected by a microplate reader at 570 nm.

2.7. Fingerprintings based on g-CDs@MMT composites

Tinfoil, glass and plastic were used to collect fingerprints, and g-CDs@MMT composites were used as fluorescent labeling makers. Before preparing the fingerprints, the hands of donors were thoroughly washed in water and dried by a hairdryer. The fingers were then pressed onto the tinfoil, glass and plastic to prepare the fingerprint samples, which were allowed to dry in the ambient atmosphere for 1–2 min. Finally, the g-CDs@MMT composites were sprinkled onto the fingerprint samples, and the superfluous power was brushed with a brush. Latent fingerprint detection under UV light showing green emission was then realized.

2.8. Characterization

PL spectra and UV–visible absorption spectra were collected by a Hitachi F-7000 spectrophotometer and a Shimadzu UV-3010 PC spectrophotometer, respectively. The calibrated integrating sphere in an FLS920 spectrometer was used to calculate the photoluminescence quantum yields (PLQYs) of the g-CDs solutions and the g-CDs@MMT composites under 405 nm excitation. The photostability of the g-CDs@MMT composites and commercial fluorescein sodium were tested through continuously irradiating these samples with a 15 W mercury lamp equipped with a 450 nm short wave pass filter (power density: 1.6 $W \cdot cm^{-2}$) at ambient room temperature; each measurement was taken three times. Transmission electron microscopy (TEM) was carried out with a Hitachi H-800 electron microscope, and a JEOL FESEM 6700F electron microscope with a primary electron energy of 3 kV was used for scanning electron microscopy (SEM) of the g-CDs@MMT composites. X-ray photoelectron spectroscopy (XPS) was conducted on a VG ESCALAB MKII spectrometer with Mg KR excitation (1253.6 eV). The binding energy calibration was based on C 1s at 284.6 eV. Fourier transform infrared (FTIR) spectra were obtained on a Nicolet AVATAR 360 FTIR instrument. The zeta potential measurements were performed on a Zetasizer Nano-ZS (Malvern Instruments). The energy dispersive spectra (EDS) and the elemental mapping of the g-CDs@MMT composites were carried out using an Inca X-Max instrument (Oxford instruments), and X-ray powder diffraction (XRD) of the g-CDs@MMT composites was recorded by a Siemens D5005 diffractometer. A single lensreflex camera (Nikon D70) and C2+ confocal microscope system (Nikon Confocal Instruments) were used to obtain images of the products and the fluorescence microscopy images of the g-CDs@MMT composites, respectively.

3. Results and discussion

The g-CDs were synthesized from citric acid and urea by a microwave-assisted heating method according to our previous work [52]. During this process, citric acid and urea are joined by dehydration condensation and subsequent carbonization to form the g-CDs. As seen from Fig. S1, the aqueous solution of g-CDs presents faint yellow color under sunlight, while under ultraviolet (UV) light it gives a strong green luminescence. The UV–vis absorption peak of the g-CDs aqueous solution was centered at 410 nm, which demonstrates a strong blue light absorption. The PL emission spectrum of the g-CDs aqueous solution showed a peak located at 522 nm under 405 nm light, with PLQYs of 14% (Fig. S1).

To achieve stable and strong luminescent materials of g-CDs in a solid state, the g-CDs were joined with MMT clays to prevent g-CD aggregation, because solid-state g-CD could induce luminescence quenching. The g-CDs were dissolved in 20 mL of aqueous solution, and MMT clay was dispersed in aqueous solution to form a turbid liquid. The g-CDs aqueous solution was then mixed with the MMT clay solution. During this process, g-CDs interact with the MMT clay layers through multifactor interactions (discussed later), finally leading to the formation of g-CDs@MMT composites (Fig. 1). In this convenient approach, g-CDs@MMT composites are easily and quickly prepared. To optimize the quality of the g-CDs@MMT composites, composites with various preparation times were obtained by changing the mixing times of the g-CDs and MMT (0.5, 4, 8, and 24 h). Their PL emission spectra and PLQYs were nearly identical (Figs. 2c and S2), indicating that a mixing time of 30 min was sufficient to allow optimum access of the g-CDs into MMT. As shown in Fig. 2a and b, under sunlight the composites presented as faint yellow powders. When irradiated by UV light, the g-CDs@MMT composites emitted a bright green fluorescence from the g-CDs, whereas MMT clay alone had no PL emission

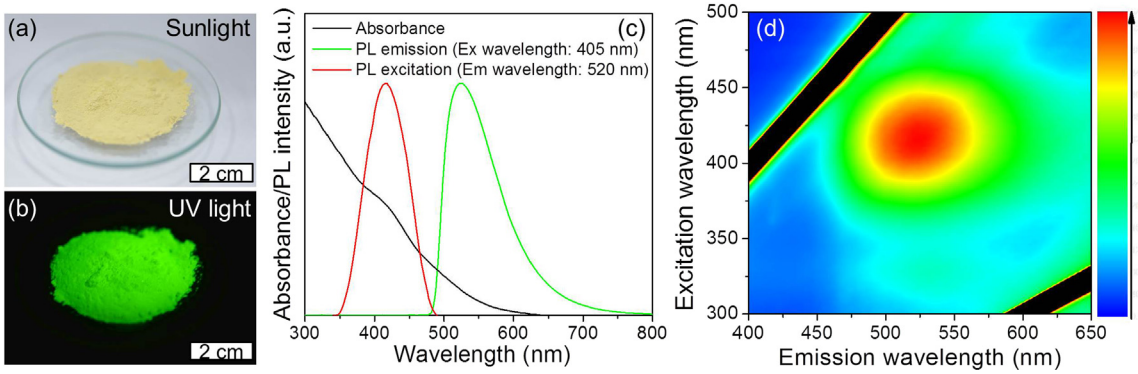

Fig. 2. The images of g-CDs@MMT composites synthesized by mixing g-CDs and MMT for 30 min under (a) sunlight and (b) UV light. (c) The absorption, PL emission and PL excitation spectra of g-CDs@MMT composites. (d) Excitation-emission maps of g-CDs@MMT composites.

under UV light (Fig. S3). Moreover, the mass ratio of g-CDs to MMT in the composites can be easily adjusted by varying the initial concentration of g-CD aqueous solution (Figs. S4 and S5). Fig. 2c shows the absorption, PL emission and PL excitation spectra of the g-CDs@MMT composites, with the PL peak located at 525 nm under 405 nm light excitation and PLQYs of 11%, which is a slightly lower than that of the g-CDs aqueous solution. The reduced PLQYs are mainly due to the presence of a small number of metal cations in the composites (Fig. 3d), which could slightly deteriorate the PL property of the g-CDs [55]. This conclusion can be further demonstrated by comparing the PL decay curves of the g-CDs and the g-CDs@MMT composites (Fig. S6). As seen from Fig. S6, the luminescence lifetime of the g-CDs@MMT composites (4.75 ns) is shorter than that of the g-CD solution (5.95 ns), indicating that the nonradiative recombination rate in the composites is somehow higher compared with that of the g-CDs solution, leading to the reduced PLQYs. Nevertheless, the g-CDs@MMT composites with PLQYs of 11% are still able to be used in LEDs according to our previous studies [56]. By comparing the excitation-emission maps of the g-CD aqueous solution and the g-CDs@MMT composites, it was found that these two matrixes were similar, indicating the successful incorporation of g-CDs into MMT (Figs. 2d and S1b).

To investigate the mechanism of the association between the g-CDs and MMT during the fabrication of the composites, analyses of the zeta potential, Fourier transform infrared (FTIR) spectra, and X-ray photoelectron spectroscopy (XPS) were carried out. In our

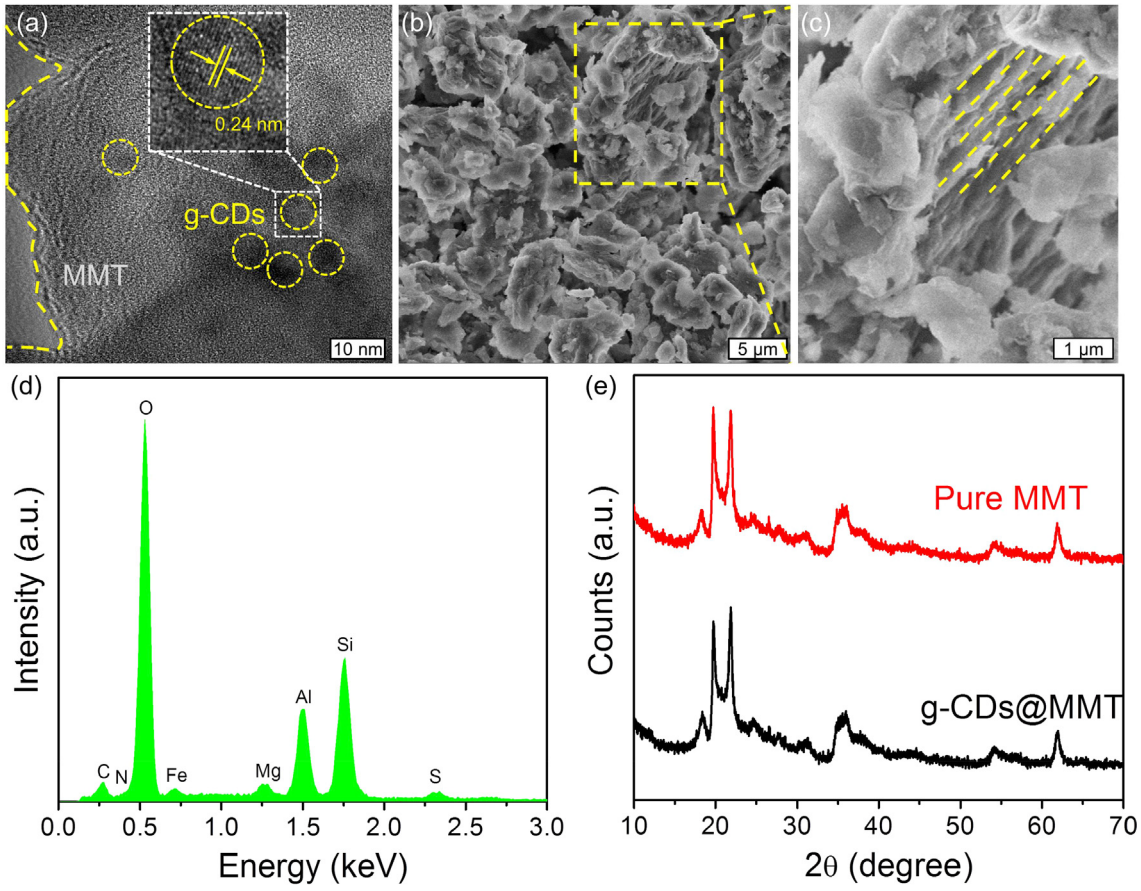

Fig. 3. (a) HRTEM image, (b and c) SEM images, and (d) EDS pattern of the g-CDs@MMT composites. (e) XRD patterns of the g-CDs@MMT composites (black line) and pure MMT (red line). (For interpretation of the references to colour in this figure legend, the reader is referred to the web version of this article.)

previous work, the zeta potential of g-CDs in aqueous solution was measured to be −32 mV [52], and the negative potential was mainly due to the presence of many carboxyl and hydroxyl groups on the g-CD surface, which was also confirmed by FTIR and XPS (Figs. S7 and S8). On the other hand, the zeta potential of MMT in aqueous solution was measured to be 37 mV (Fig. S9). Therefore, there is electrostatic attraction between g-CDs and MMT, promoting their association. In addition to electrostatic attraction, further FTIR and XPS characterization found that there are other interactions, including hydrogen bonding and complexation. As shown in Fig. S7, the FTIR spectrum of g-CDs exhibits a C=O stretching vibration at 1700 cm^{-1} along with O—H/N—H stretching vibration, indicating the presence of carboxyl and hydroxyl groups. MMT presents Al—OH bending vibration at 917 cm^{-1}, Si—O stretching vibration at 1029 cm^{-1}, O—H bending vibration at 1390 and 1634 cm^{-1}, and O—H stretching vibration, showing that there are many hydroxyl groups in the MMT clays. Therefore, hydrogen bonds could be formed between the carboxyl/hydroxyl groups of the g-CDs and the hydroxyl groups of MMT during composites fabrication. Another interaction, complexation between g-CDs and MMT was confirmed by XPS analysis (Fig. S8). In the g-CD XPS spectrum, the C 1s and O 1s spectra prove the existence of the carboxyl and hydroxyl groups, and these groups could interact with the metal cations that are present in the MMT clay clays (i.e., Al) through complexation. Compared to pure MMT, the peak of Al 2p in the composites was shifted to a lower binding energy, which should be ascribed to the coordination effect between the Al in MMT and the carboxyl/hydroxyl groups in the g-CDs. The carboxyl/hydroxyl groups in g-CDs could provide Al with electrons, which increase the electron cloud density of Al, resulting in a decreased Al binding energy. In addition, since there are no C elements in MMT, the presence of C elements in the g-CDs@MMT composites

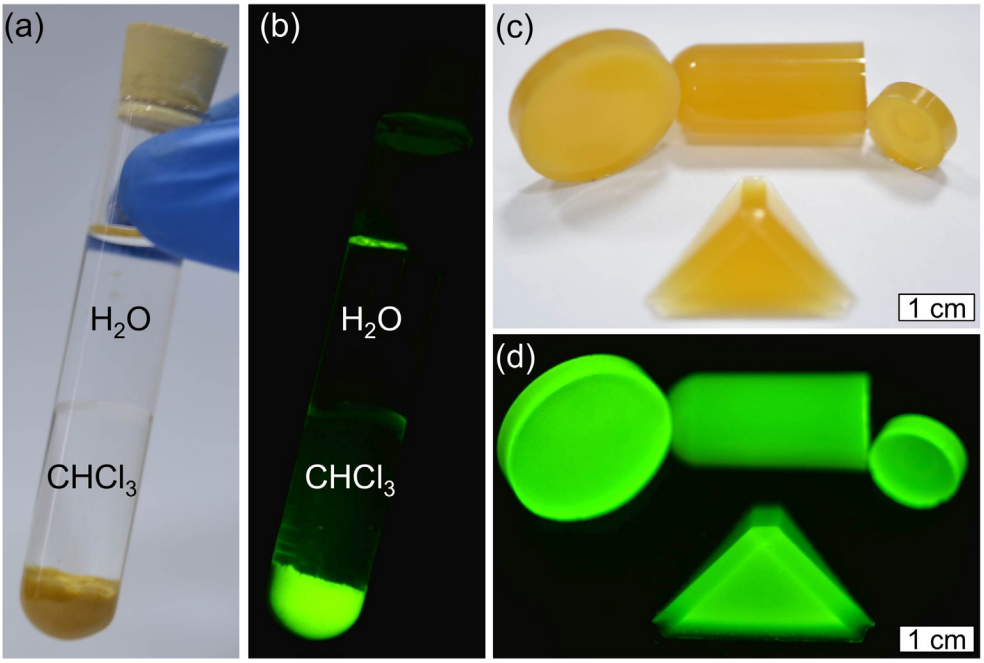

Fig. 4. (a) Optical image and (b) fluorescent image of the g-CDs@MMT composites in $CHCl_3$. The images of luminescent bulks, which are composed of g-CDs@MMT composites and epoxy-silicone resin, are taken under (c) sunlight and (d) UV light.

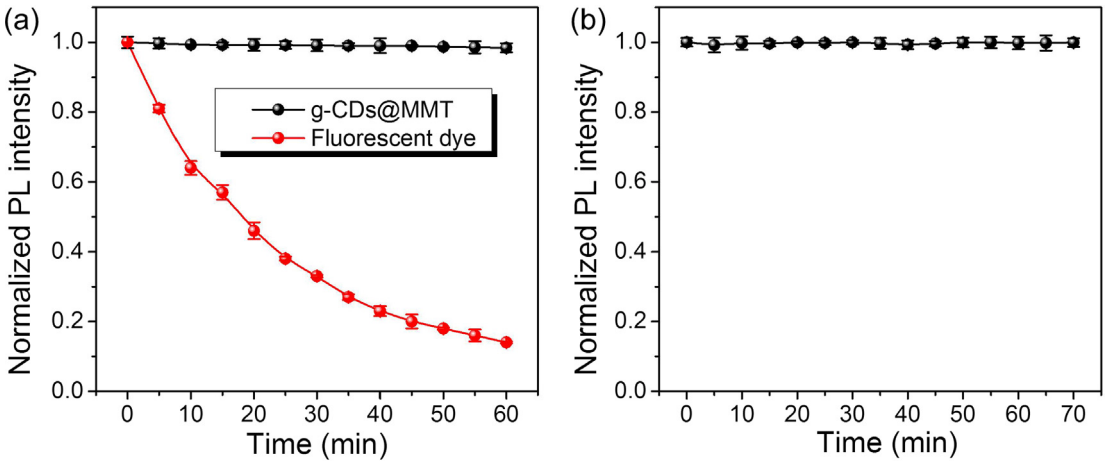

Fig. 5. (a) The decay curves of the PL intensity of the g-CDs@MMT composites (black spheres) and fluorescent dye (red spheres) under UV light (1.6 $W{\cdot}cm^{-2}$) with the same conditions. (b) The variation of PL intensity of a bulk material, prepared by mixing the composites and the epoxy-silicone resin and subsequently heating the mixture, was measured at 85 °C. The error bars are based on three repeat experiments. (For interpretation of the references to colour in this figure legend, the reader is referred to the web version of this article.)

further proves the successful loading of g-CDs into MMT (Fig. S8e). Over, the association of g-CDs and MMT in preparing the g-CDs@MMT composites is based on multifactor interaction, including electrostatic attraction, hydrogen bonding and complexation.

To further characterize the structure, morphology and composition of g-CDs@MMT composites, high-resolution transmission electron microscopy (HRTEM), scanning electron microscopy (SEM), energy dispersive spectra (EDS) and X-ray powder diffraction (XRD) studies were carried out. In the HRTEM and SEM images of pure MMT, there were no g-CDs present (Fig. S10). In contrast, the HRTEM image in Fig. 3a shows that the structure of g-CDs@MMT composites is layered and the g-CDs are dispersed within the layers without obvious aggregation. The lattice spacing of g-CDs in the HRTEM image is 0.24 nm, which is consistent with the (1 1 0) lattice plans of graphitic carbon [48]. As shown in Fig. 3b and c, SEM images further revealed that g-CDs@MMT composites are layered structure. The layered stripes, which are marked by the yellow dotted lines in Fig. 3c, are clearly visible in the high-resolution SEM images. Based on the EDS spectrum (Fig. 3d), the g-CDs@MMT composites are composed of eight elements, including C, N, O, Fe, Mg, Al, Si and S. Of these, a portion of the C, N and O belongs to the g-CDs, whereas S, Fe, Mg and Al originate from MMT clays. In addition, the EDS analysis confirmed that PLQYs of g-CDs@MMT composites are indeed affected by metal elements. According to the HRTEM, SEM and EDS analysis the g-CDs are certainly embedded into the MMT clay layers. Furthermore, the XRD pattern of g-CDs@MMT composites is consistent with that of pure MMT clays (Fig. 3e). For the g-CDs, there are no significant single peaks in the XRD pattern because they are weak and overlapped by those of MMT [52].

Due to the good stability of g-CDs and the protection of the MMT clays, g-CDs@MMT composites also possess the ability to resist organic solvents. As shown in Fig. S11, the g-CDs remained undissolved in chloroform, maintaining an aggregated state that cause fluorescence quenching. Under UV light, the chloroform solution containing the g-CDs had almost no photoluminescence. After treatment with chloroform, the g-CDs were dried in an oven and then dissolved in deionized water. Their absorption spectra and PL emission spectra were identical to those of untreated g-CDs in aqueous solution. Similarly, Fig. 4a and b shows that the g-CDs@MMT composites were not dissolved or swollen in chloroform. Under UV light excitation, g-CDs@MMT composites can stably emit strong green luminescence (Fig. 4b). Due to the excellent resistance to organic solvent, g-CDs@MMT composites can be mixed with epoxy-silicone resin A and B, which are types of commercial packing materials, to form luminescent bulk materials (Fig. 4c and d). The resultant strongly luminescent bulk materials

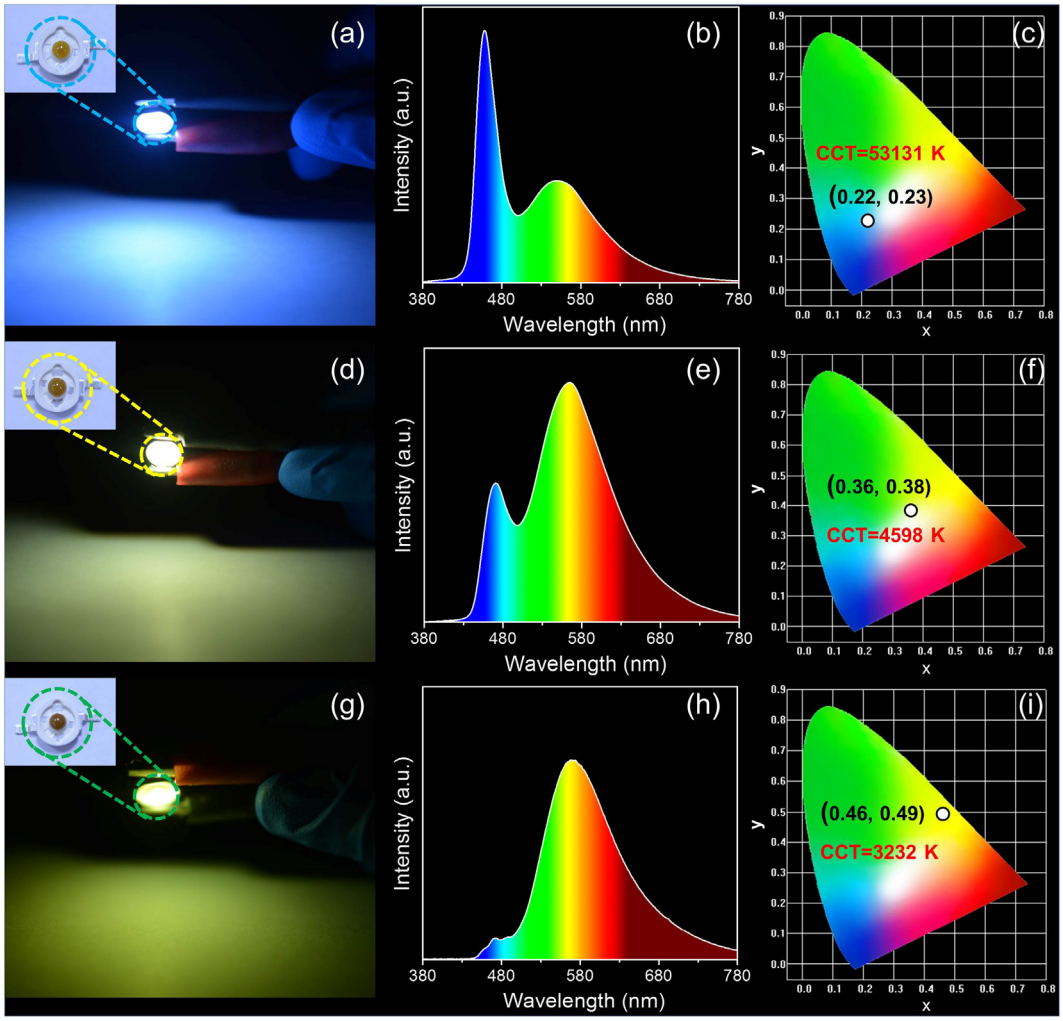

Fig. 6. Images of working WLEDs with different CIE coordinates and color temperatures. The volume ratios of g-CDs@MMT composites to epoxy-silicone resin are (a) 4:3, (d) 5:3 and (g) 8:3. The corresponding spectra of WLEDs are shown in (b), (e) and (h). The detailed CIE coordinates and color temperature are shown in (c), (f) and (i). (For interpretation of the references to colour in this figure legend, the reader is referred to the web version of this article.)

can be easily molded into different shapes (Fig. 4c). Under UV light excitation, the bulk materials show green emission, which is consistent with the g-CDs@MMT composites (Fig. 2b and d). The homogeneous emissions from the whole bulk materials suggest a good distribution of the composites within the packing materials, which is ascribed to the pulverulent state of the composites (Figs. 3b and 4d).

Meanwhile, g-CDs@MMT composites have excellent photostability under UV light, as do g-CDs. At ambient room temperature, a UV light (15 W mercury lamp equipped with a 450 nm short-wave pass filter; power density: 1.6 $W{\cdot}cm^{-2}$) was used to compare the photostability of g-CDs@MMT composites with commercial fluorescein sodium which is a common fluorescent dye. As seen from Fig. 5a, when irradiated by UV light, the PL intensities of all samples underwent deterioration. The PL intensity of fluorescent dye decreased at a very fast rate. In the first 5 min, the PL intensity decreased by more than 20%. After 20 min, the PL intensity decreased below 50% of its initial intensity. When irradiated for 60 min, its PL intensity further decreased by more than 80%. Finally, less than 20% of the PL intensity was retained. However, the PL intensity of the g-CDs@MMT composites was maintained in a stable state. When continuously irradiated by UV light for 60 min, the PL intensity of the g-CDs@MMT composites was maintained at approximately 98%. According to our previous study, the temperature of LEDs at the working voltage is approximately 85 °C [57]. At this temperature, the g-CDs have good stability (Fig. S12); therefore, the g-CDs@MMT composites are expected to exhibit excellent thermal stability. To verify the potential of using g-CDs@MMT composites in LEDs, a bulk material (shown in Fig. 4d) was first prepared by mixing the composites and the epoxy-silicone resin; then the PL intensity of the bulk materials was monitored *in situ* at 85 °C for 70 min (Fig. 5b). After 70 min of heating, the PL intensity of the bulk materials containing g-CDs@MMT composites was nearly unchanged, indicating the great potential of applying g-CDs@MMT composites in LEDs as a color conversion layer. Importantly, the g-CDs@MMT composites have low toxicity, primarily because the component g-CDs and MMT also have low toxicity, as demonstrated by toxicity assays (Fig. S13). RAW264.7 cells were selected to test the cytotoxicity mainly because these cells can phagocytize foreign materials. This phagocytic behavior can be used to better evaluate the toxicity of the materials inside the cell. Therefore, all of the aforementioned advantages, including excellent photostability, thermal stability, resistance to organic solvent, and small particle sizes, ensure the further applications of g-CDs@MMT composites in LEDs upon mixing with commercial packing materials and in latent fingerprint detection.

White LEDs (WLEDs) (Fig. 6) could be fabricated based on g-CDs@MMT composites and a blue-emitting chip with 450 nm emission (Fig. S14). First, g-CDs@MMT composites were mixed with epoxy-silicon resin A and B, and the mixture was then applied as a conversion layer in fabricating the WLEDs by depositing on the blue-emitting chips. The WLEDs were then placed in an oven at 80 °C for 1 h to solidify. By adjusting the amount of g-CDs@MMT composites, WLEDs with different CIE coordinates and color temperatures are obtained. As seen in Fig. 6, the mass ratios of

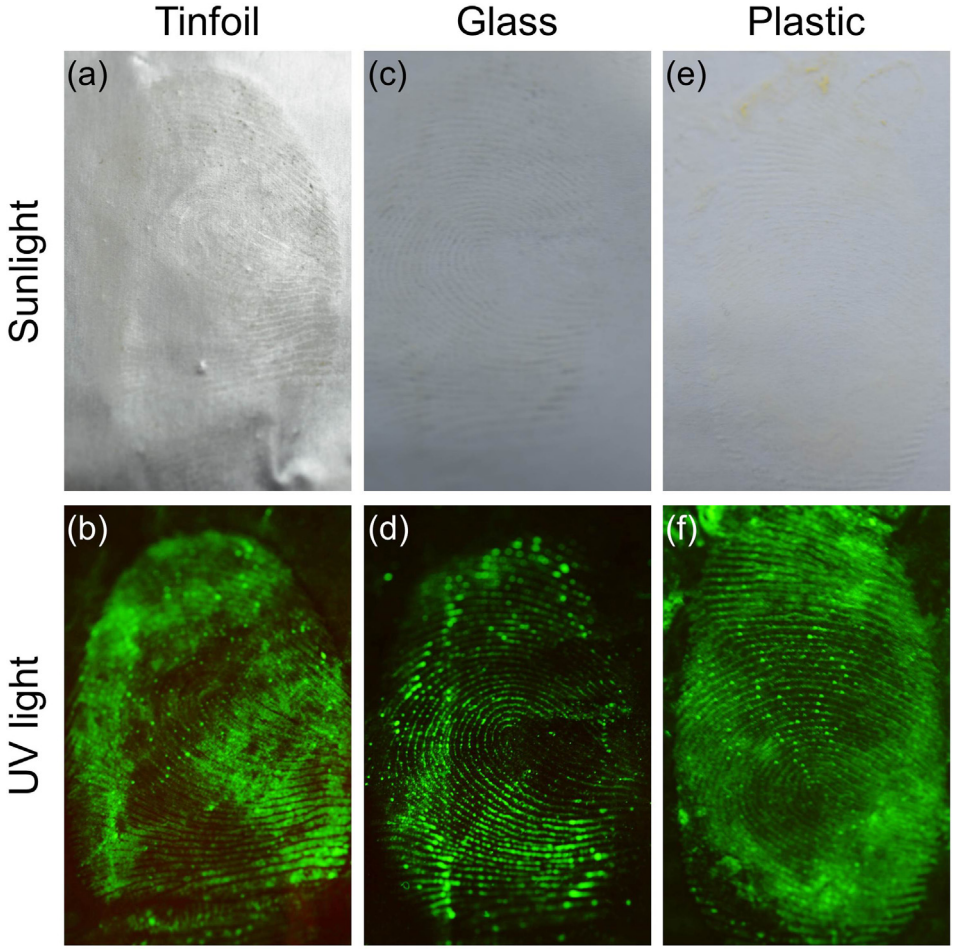

Fig. 7. Latent fingerprints detection images taken under (a–c) sunlight and (d–f) UV light using g-CDs@MMT composites as the fluorescent labeling markers on a variety of substances tinfoil (a and d), glass (c and d) and plastic (e and f).

the g-CDs@MMT composites and epoxy-silicon resin ranged from 8:3 to 4:3, and three different samples were fabricated. Fig. 6d shows a WLED with CIE coordinates of (0.36, 0.38) and color temperature of 4598 K. By reducing the amount of g-CDs@MMT composites, a cool WLED with CIE coordinates of (0.22, 0.23) and a color temperature of 53131 K was achieved (Fig. 6a and c). Conversely, by increasing the g-CDs@MMT composites concentration, a warm WLED was realized, whose CIE coordinate and color temperature were (0.46, 0.49) and 3232 K, respectively (Fig. 6g and i). The variations in LED color temperature when changing composite-epoxy-silicon resin ratio is due to reabsorption among the g-CDs. Because there is an overlap between the PL emission and absorbance of the g-CDs@MMT composites (Fig. 2b), reabsorption can occur due to the energy emission along the light transmission path.[52] When adjusting the mass ratios of composites and resin, reabsorption could clearly be observed, This phenomena could also be demonstrated by the LED PL emission spectra (Fig. 6b, e and h), resulting in a red shift of the emission peaks. The reabsorption process could be further proved by measuring the PL emission spectra of three bulk materials with various composite-to-resin ratios (1:18, 1:6, and 1:4). As shown in Fig. S15, as the composite-to-resin ratio increased, the reabsorption process becomes stronger, resulting in an obvious red shift of 54 nm and low emission efficiency. Furthermore, due to the good photostability of the g-CDs@MMT composites (Fig. 5a), the fabricated WLEDs are quite stable (Fig. S16). After continuously working for three weeks, the emission intensity of the WLEDs was nearly unchanged, indicating the usability of the g-CDs@MMT composites in real-world systems and applications.

The g-CDs@MMT composites can also be used to collect fingerprints in the areas of healthcare and forensic science. Fig. 7 displays the images of fingerprints by using g-CDs@MMT composites as a fluorescent labeling marker on various materials, such as tinfoil, glass and plastic. Fig. 7a, c and e shows the fingerprints on tinfoil, glass and plastic under sunlight, respectively. Under UV light, it is clear that the green-emissive fingerprints are well detected without background staining, including finger ridge details (Fig. 7b, d and f). The clear fingerprints without background staining indicate that the g-CDs@MMT composites can be adhered by the residual oil in human skin, whereas almost no composites are located in the area without a fingerprint, leading to the enhancement of the signal-to-noise ratio. Moreover, the application of g-CDs@MMT composites efficiently avoids the diffusion of liquid fluorescent labeling markers on the surfaces, which is a unique advantage. Hence, using g-CDs@MMT composites as fluorescent labeling markers for latent fingerprint detection is a significant area of application.

4. Conclusions

Solid-state highly photoluminescent materials are highly sought after for the development of high-performance LEDs and for use in latent fingerprint detection [1,5,6]. Although various solid-state photoluminescent materials, such as rare earth-doped nanoparticles, organic dyes, semiconductor QDs and perovskites QDs, have been explored, some limitations remain in their application, including the inability to be regenerate, weak thermostability, and potential toxicity [21–25]. Thus, the exploration of novel solid-state luminescent materials has attracted increasing attention. This work, along with previous studies, indicates that latent fingerprint detection and WLEDs with tunable CIE coordinates and color temperature can be realized by applying g-CDs@MMT composites [22,42,52,53]. The role of MMT clay during the process of preparing g-CDs@MMT composites is to prevent g-CD aggregation, maintaining the fluorescence of g-CDs in the solid state. Furthermore, through zeta potential, FTIR and XPS characterizations, the synthesis of the g-CDs@MMT composites has been shown to be based on multifactor interactions, including electrostatic attraction, hydrogen bonding and complexation. Through these strong interactions, g-CDs@MMT composites were fabricated and had a PL peak position at 525 nm and PLQYs of 11% at 405 nm excitation. Due to the properties of the MMT clay, the g-CDs@MMT composites exhibited photo-stability, thermostability and resistance to solvents. After continuous UV irradiations for 60 min and storage at 85 °C for 70 min, the PL intensity of the g-CDs@MMT composites could be preserved at 98% and 100%, respectively. All of the abovementioned advantages allow g-CDs@MMT composites to be used as a conversion layer in WLEDs. By adjusting the amount of g-CDs@MMT composites, WLEDs with tunable CIE coordinates and color temperature could be fabricated, and the fabricated WLEDs were able to continuously work for five hundreds hours without changes in the emission intensity. In addition, g-CDs@MMT composites have smaller particle sizes. This allows them to be used for fingerprint collection in healthcare and forensic science applications. These findings contribute new insights into the novel design of CDs-based luminescent materials, broadening the possibilities for CD applications.

Author contributions

The manuscript was written through contributions of all authors. All authors have given approval to the final version of the manuscript.

Acknowledgment

This work is supported by the National Natural Science Foundation of China (projects No. 51602304, 81600879), Jilin Province Science and Technology Research (projects No. 20190103088JH, 20180520010JH, 20150519003JH, 20140101060JC, 20170101191JC, 20170101042JC), Young Elite Scientist Sponsorship Program by CAST (projects No. 2018QNRC001), the Jilin Province Education Department Science and Technology Research (projects No. JJKH20190106KJ, JJKH20181026KJ), and China Postdoctoral Science Foundation (projects No. 2018T110259, 2016M601386).

Appendix A. Supplementary material

Supplementary data to this article can be found online at https://doi.org/10.1016/j.jcis.2019.07.022.

References

[1] E. Danielson, J.H. Golden, E.W. McFarland, C.M. Reaves, W.H. Weinberg, X.D. Wu, A combinatorial approach to the discovery and optimization of luminescent materials, Nature 389 (1997) 944–948.
[2] R.L. Liu, D.Q. Wu, S.H. Liu, K. Koynov, W. Knoll, Q. Li, An aqueous route to multicolor photoluminescent carbon dots using silica spheres as carriers, Angew. Chem., Int. Ed. 48 (2009) 4598–4601.
[3] M. Heiss, Y. Fontana, A. Gustafsson, G. Wüst, C. Magen, D.D. O'Regan, J.W. Luo, B. Ketterer, S. Conesa-Boj, A.V. Kuhlmann, J. Houel, E. Russo-Averchi, J.R. Morante, M. Cantoni, N. Marzari, J. Arbiol, A. Zunger, R.J. Warburton, A. Fontcuberta i Morral, Self-assembled quantum dots in a nanowire system for quantum photonics, Nat. Mater. 12 (2013) 439–444.
[4] N.Q. Gong, X.W. Ma, X.X. Ye, Q.F. Zhou, X.A. Chen, X.L. Tan, S.K. Yao, S.D. Huo, T. B. Zhang, S.Z. Chen, X.C. Teng, X.X. Hu, J. Yu, Y.L. Gan, H.D. Jiang, J.H. Li, X.J. Liang, Carbon-dot-supported atomically dispersed gold as a mitochondrial oxidative stress amplifier for cancer treatment, Nat. Nanotechnol. (2019), https://doi.org/10.1038/s41565-41019-40373-41566.
[5] V.L. Colvin, M.C. Schlamp, A.P. Alivisatos, Light-emitting diodes made from cadmium selenide nanocrystals and a semiconducting polymer, Nature 370 (1994) 354–357.
[6] N. Grandjean, R. Butté, Solid-state lighting on glass, Nat. Photon. 5 (2011) 714–715.

[7] Y. Xiong, J. Schneider, E.V. Ushakova, A.L. Rogach, Influence of molecular fluorophores on the research field of chemically synthesized carbon dots, Nano Today 23 (2018) 124–139.
[8] J.C. Liu, N. Wang, Y. Yu, Y. Yan, H.Y. Zhang, J.Y. Li, J.H. Yu, Carbon dots in zeolites: A new class of thermally activated delayed fluorescence materials with ultralong lifetimes, Sci. Adv. 3 (2017) e1603171.
[9] M. Fröbel, T. Schwab, M. Kliem, S. Hofmann, K. Leo, M.C. Gather, Get it white: color-tunable AC/DC OLEDs, Light: Sci. Appl. 4 (2015) e247.
[10] Y.F. Wang, A.G. Hu, Carbon quantum dots: synthesis, properties and applications, J. Mater. Chem. C 2 (2014) 6921–6939.
[11] A.W. Zhu, Q. Qu, X.L. Shao, B. Kong, Y. Tian, Carbon-dot-based dual-emission nanohybrid produces a ratiometric fluorescent sensor for in vivo imaging of cellular copper ions, Angew. Chem., Int. Ed. 51 (2012) 7185–7189.
[12] B.Q. Liu, L. Wang, D.Y. Gao, J.H. Zou, H.L. Ning, J.B. Peng, Y. Cao, Extremely high-efficiency and ultrasimplified hybrid white organic light-emitting diodes exploiting double multifunctional blue emitting layers, Light: Sci. Appl. 5 (2016) e16137.
[13] A.L. Rogach, N. Gaponik, J.M. Lupton, C. Bertoni, D.E. Gallardo, S. Dunn, N.L. Pira, M. Paderi, P. Repetto, S.G. Romanov, C. O'Dwyer, C.M.S. Torres, A. Eychmüller, Light-emitting diodes with semiconductor nanocrystals, Angew. Chem., Int. Ed. 47 (2008) 6538–6549.
[14] J. Lee, V.C. Sundar, J.R. Heine, M.G. Bawendi, K.F. Jensen, Full color emission from II-VI semiconductor quantum dot-polymer composites, Adv. Mater. 12 (2000) 1102–1105.
[15] I. Dursun, C. Shen, M.R. Parida, J. Pan, S.P. Sarmah, D. Priante, N. Alyami, J.K. Liu, M.I. Saidaminov, M.S. Alias, A.L. Abdelhady, T.K. Ng, O.F. Mohammed, B.S. Ooi, O.M. Bakr, Perovskite nanocrystals as a color converter for visible light communication, ACS Photonics 3 (2016) 1150–1156.
[16] Y.J. Chang, X.D. Yao, Z.P. Zhang, D.L. Jiang, Y.L. Yu, L.F. Mi, H. Wang, G.P. Li, D.B. Yu, Y. Jiang, Preparation of highly luminescent $BaSO_4$ protected CdTe quantum dots as conversion materials for excellent color-rendering white LEDs, J. Mater. Chem. C 3 (2015) 2831–2836.
[17] Z.J. Zhou, P.F. Tian, X.Y. Liu, S.L. Mei, D. Zhou, D. Li, P.T. Jing, W.L. Zhang, R.Q. Guo, S.N. Qu, A.L. Rogach, Hydrogen peroxide-treated carbon dot phosphor with a bathochromic-shifted, aggregation-enhanced emission for light-emitting devices and visible light communication, Adv. Sci. 1800369 (2018).
[18] G. Lozano, D.J. Louwers, S.R.K. Rodríguez, S. Murai, O.T.A. Jansen, M.A. Verschuuren, J. Gómez Rivas, Plasmonics for solid-state lighting: Enhanced excitation and directional emission of highly efficient light sources, Light: Sci. Appl. 2 (2013) e66.
[19] X.F. Li, J.D. Budai, F. Liu, J.Y. Howe, J.H. Zhang, X.J. Wang, Z.J. Gu, C.J. Sun, R.S. Meltzer, Z.W. Pan, New yellow $Ba_{0.93}Eu_{0.07}Al_2O_4$ phosphor for warm-white light-emitting diodes through single-emitting-center conversion, Light: Sci. Appl. 2 (2013) e50.
[20] P.P. Dai, C. Li, X.T. Zhang, J. Xu, X. Chen, X.L. Wang, Y. Jia, X.J. Wang, Y.C. Liu, A single Eu^{2+}-activated high-color-rendering oxychloride white-light phosphor for white-light-emitting diodes, Light: Sci. Appl. 5 (2016) e16024.
[21] Q.Q. Dai, C.E. Duty, M.Z. Hu, Semiconductor-nanocrystals-based white light-emitting diodes, Small 6 (2010) 1577–1588.
[22] Y.C. Zhai, Y. Wang, D. Li, D. Zhou, P.T. Jing, D.Z. Shen, S.N. Qu, Red carbon dots-based phosphors for white light-emitting diodes with color rendering index of 92, J. Colloid Interface Sci. 528 (2018) 281–288.
[23] S.H. Lim, Y.H. Ko, C. Rodriguez, S.H. Gong, Y.H. Cho, Electrically driven, phosphor-free, white light-emitting diodes using gallium nitride-based double concentric truncated pyramid structures, Light: Sci. Appl. 5 (2016) e16030.
[24] S. Abe, J.J. Joos, L.I.D.J. Martin, Z. Hens, P.F. Smet, Hybrid remote quantum dot/powder phosphor designs for display backlights, Light: Sci. Appl. 6 (2017) e16271.
[25] E. Jang, S. Jun, H. Jang, J. Lim, B. Kim, Y. Kim, White-light-emitting diodes with quantum dot color converters for display backlights, Adv. Mater. 22 (2010) 3076–3080.
[26] J.C. Ge, Q.Y. Jia, W.M. Liu, L. Guo, Q.Y. Liu, M.H. Lan, H.Y. Zhang, X.M. Meng, P.F. Wang, Red-emissive carbon dots for fluorescent, photoacoustic, and thermal theranostics in living mice, Adv. Mater. 27 (2015) 4169–4177.
[27] C.J. Reckmeier, J. Schneider, A.S. Susha, A.L. Rogach, Luminescent colloidal carbon dots: optical properties and effects of doping [invited], Opt. Express 24 (2016) A312–A340.
[28] S. Chaudhary, A. Umar, K.K. Bhasin, S. Singh, Applications of carbon dots in nanomedicine, J. Biomed. Nanotechnol. 13 (2017) 591–637.
[29] M.L. Liu, B.B. Chen, C.M. Li, C.Z. Huang, Carbon dots: synthesis, formation mechanism, fluorescence origin and sensing applications, Green Chem. 21 (2019) 449–471.
[30] H. Ding, S.B. Yu, J.S. Wei, H.M. Xiong, Full-color light-emitting carbon dots with a surface-state-controlled luminescence mechanism, ACS Nano 10 (2016) 484–491.
[31] C. Sun, Y. Zhang, S. Kalytchuk, Y. Wang, X.Y. Zhang, W.Z. Gao, J. Zhao, K. Cepe, R. Zboril, W.W. Yu, A.L. Rogach, Down-conversion monochromatic light-emitting diodes with the color determined by the active layer thickness and concentration of carbon dots, J. Mater. Chem. C 3 (2015) 6613–6615.
[32] P. Zhao, X.P. Li, G. Baryshnikov, B. Wu, H. Ågren, J.J. Zhang, L.L. Zhu, One-step solvothermal synthesis of high-emissive amphiphilic carbon dots *via* rigidity derivation, Chem. Sci. 9 (2018) 1323–1329.
[33] Y.J. Zhang, R.R. Yuan, M.L. He, G.C. Hu, J.T. Jiang, T. Xu, L. Zhou, W. Chen, W.D. Xiang, X.J. Liang, Multicolour nitrogen-doped carbon dots: tunable photoluminescence and sandwich fluorescent glass-based light-emitting diodes, Nanoscale 9 (2017) 17849–17858.
[34] S.K. Kailasa, S. Ha, S.H. Baek, L.M.T. Phan, S. Kim, K. Kwak, T.J. Park, Tuning of carbon dots emission color for sensing of Fe^{3+} ion and bioimaging applications, Mater. Sci. Eng., C 98 (2019) 834–842.
[35] M.L. Desai, H. Basu, R.K. Singhal, S. Saha, S.K. Kailasa, Ultra-small two dimensional MXene nanosheets for selective and sensitive fluorescence detection of Ag^+ and Mn^{2+} ions, Colloids Surf., A 565 (2019) 70–77.
[36] J.R. Bhamore, S. Jha, T.J. Park, S.K. Kailasa, Green synthesis of multi-color emissive carbon dots from manilkara zapota fruits for bioimaging of bacterial and fungal cells, J. Photochem. Photobiol., B 191 (2019) 150–155.
[37] J.R. Bhamore, S. Jha, T.J. Park, S.K. Kailasa, Fluorescence sensing of Cu^{2+} ion and imaging of fungal cell by ultra-small fluorescent carbon dots derived from acacia concinna seeds, Sens. Actuat., B 277 (2018) 47–54.
[38] V.N. Mehta, S. Jha, S.K. Kailasa, One-pot green synthesis of carbon dots by using saccharum officinarum juice for fluorescent imaging of bacteria (escherichia coli) and yeast (saccharomyces cerevisiae) cells, Mater. Sci. Eng., C 38 (2014) 20–27.
[39] K. Jiang, S. Sun, L. Zhang, Y. Lu, A.G. Wu, C.Z. Cai, H.W. Lin, Red, green, and blue luminescence by carbon dots: Full-color emission tuning and multicolor cellular imaging, Angew. Chem., Int. Ed. 54 (2015) 5360–5363.
[40] D. Qu, M. Zheng, J. Li, Z.G. Xie, Z.C. Sun, Tailoring color emissions from N-doped graphene quantum dots for bioimaging applications, Light: Sci. Appl. 4 (2015) e364.
[41] X.D. Yang, X. Yang, Z.Y. Li, S.Y. Li, Y.X. Han, Y. Chen, X.Y. Bu, C.Y. Su, H. Xu, Y.N. Jiang, Q. Lin, Photoluminescent carbon dots synthesized by microwave treatment for selective image of cancer cells, J. Colloid Interface Sci. 456 (2015) 1–6.
[42] D. Zhou, D. Li, P.T. Jing, Y.C. Zhai, D.Z. Shen, S.N. Qu, A.L. Rogach, Conquering aggregation-induced solid-state luminescence quenching of carbon dots through a carbon dots-triggered silica gelation process, Chem. Mater. 29 (2017) 1779–1787.
[43] C. Liu, L. Bao, B. Tang, J.Y. Zhao, Z.L. Zhang, L.H. Xiong, J. Hu, L.L. Wu, D.W. Pang, Fluorescence-converging carbon nanodots-hybridized silica nanosphere, Small 12 (2016) 4702–4706.
[44] J. Chen, J.S. Wei, P. Zhang, X.Q. Niu, W. Zhao, Z.Y. Zhu, H. Ding, H.M. Xiong, Red-emissive carbon dots for fingerprints detection by spray method: Coffee ring effect and unquenched fluorescence in drying process, ACS Appl. Mater. Interfaces 9 (2017) 18429–18433.
[45] X. Guo, C.F. Wang, Z.Y. Yu, L. Chen, S. Chen, Facile access to versatile fluorescent carbon dots toward light-emitting diodes, Chem. Commun. 48 (2012) 2692–2694.
[46] X.M. Li, M.C. Rui, J.Z. Song, Z.H. Shen, H.B. Zeng, Carbon and graphene quantum dots for optoelectronic and energy devices: a review, Adv. Funct. Mater. 25 (2015) 4929–4947.
[47] B.P. Jiang, Y.X. Yu, X.L. Guo, Z.Y. Ding, B. Zhou, H. Liang, X.C. Shen, White-emitting carbon dots with long alkyl-chain structure: effective inhibition of aggregation caused quenching effect for label-free imaging of latent fingerprint, Carbon 128 (2018) 12–20.
[48] D. Zhou, P.T. Jing, Y. Wang, Y.C. Zhai, D. Li, Y. Xiong, A.V. Baranov, S.N. Qu, A.L. Rogach, Carbon dots produced via space-confined vacuum heating: Keeping efficient luminescence in both dispersed and aggregated state, Nanoscale Horiz. 4 (2019) 388–395.
[49] Y. Wang, S. Kalytchuk, L.Y. Wang, O. Zhovtiuk, K. Cepe, R. Zboril, A.L. Rogach, Carbon dot hybrids with oligomeric silsesquioxane: solid-state luminophores with high photoluminescence quantum yield and applicability in white light emitting devices, Chem. Commun. 51 (2015) 2950–2953.
[50] W. Kwon, S. Do, J. Lee, S. Hwang, J.K. Kim, S.W. Rhee, Freestanding luminescent films of nitrogen-rich carbon nanodots toward large-scale phosphor-based white-light-emitting devices, Chem. Mater. 25 (2013) 1893–1899.
[51] Y.H. Chen, M.T. Zheng, Y. Xiao, H.W. Dong, H.R. Zhang, J.L. Zhuang, H. Hu, B.F. Lei, Y.L. Liu, A self-quenching-resistant carbon-dot powder with tunable solid-state fluorescence and construction of dual-fluorescence morphologies for white light-emission, Adv. Mater. 28 (2016) 312–318.
[52] D. Zhou, Y.C. Zhai, S.N. Qu, D. Li, P.T. Jing, W.Y. Ji, D.Z. Shen, A.L. Rogach, Electrostatic assembly guided synthesis of highly luminescent carbon-nanodots@$BaSO_4$ hybrid phosphors with improved stability, Small 13 (2017) 1602055.
[53] M.Y. Sun, S.N. Qu, Z.D. Hao, W.Y. Ji, P.T. Jing, H. Zhang, L.G. Zhang, J.L. Zhao, D.Z. Shen, Towards efficient solid-state photoluminescence based on carbon-nanodots and starch composites, Nanoscale 6 (2014) 13076–13081.
[54] F. Gao, C.F. Lv, J.X. Han, X.Y. Li, Q. Wang, J. Zhang, C. Chen, Q. Li, X.F. Sun, J.C. Zheng, L.R. Bao, X. Li, CdTe–montmorillonite nanocomposites: control synthesis, UV radiation-dependent photoluminescence, and enhanced latent fingerprint detection, J. Phys. Chem. C 115 (2011) 21574–21583.
[55] Y.B. Song, S.J. Zhu, S.Y. Xiang, X.H. Zhao, J.H. Zhang, H. Zhang, Y. Fu, B. Yang, Investigation into the fluorescence quenching behaviors and applications of carbon dots, Nanoscale 6 (2014) 4676–4682.
[56] S. Liang, M. Liu, D. Zhou, H.Y. Zou, Y. Liu, X. Zhang, B. Yang, H. Zhang, Preparation of quantum dots-montmorillonite nanocomposites with strong photoluminescence for light-emitting diodes, RSC Adv. 7 (2017) 7774–7779.
[57] H.Y. Zou, M. Liu, D. Zhou, X. Zhang, Y. Liu, B. Yang, H. Zhang, Employing $CdSe_XTe_{1-x}$ alloyed quantum dots to avoid the temperature-dependent emission shift of light-emitting diodes, J. Phys. Chem. C 121 (2017) 5313–5323.